Materials Advances

ROYAL SOCIETY OF CHEMISTRY

PAPER

View Article Online
View Journal

Cite this: DOI: 10.1039/d6ma00097e

Thermodynamic studies on entropy stabilized oxide (Co,Cu,Mg,Ni,Zn)O

Florina Teodorescu,[a] Cornelia Marinescu,[a] Ancuta Sofronia,[a] Alina Botea-Petcu,[a] Cristian Hornoiu,[a] Mihail-Călin Licu,[a] Florentina Maxim,[a] David Bérardan,[b] Nita Dragoe *[b] and Speranta Tanasescu *[a]

Thermodynamic properties of the rock-salt entropy stabilized oxide (Co,Cu,Mg,Ni,Zn)O have been determined and the relevant functions suitable for evaluation of thermodynamic stability in particular temperature ranges associated with structural changes during heating have been measured. The energetic parameters obtained *via* several experimental methods under both the equilibrium and dynamic conditions (drop calorimetry, solid state electromotive force measurements, DSC/TG), together with the thermal expansion and electrical conductivity data, have been analyzed, and the relationship of the thermodynamic stability with changes in the defect structure has been revealed. Our results are consistent with a phase transition to a high entropy state around 1150 K and the large negative values of the free energy, observed in the 1173 to 1223 K temperature domain, highlight a more stable state in the sample with the rock-salt structure. The partial molar enthalpy and entropy values of oxygen dissolution in the crystalline phase increase with increasing temperature suggesting the decrease of the binding energy of oxygen and the decrease of order in the oxygen sublattice of the structure, respectively. Due to the significant increase in partial molar entropy in the temperature range of 1173–1273 K, it is likely that oxygen vacancies are not concentrated at specific oxygen sites but they are randomly distributed, supporting the previous findings related to an entropy-driven phase transformation. The experimental methods outlined in this report can be used to distinguish between the phase transitions associated with the formation of an entropy stabilized phase and highlight the correlative effects of temperature and defect structure on the thermodynamic behavior of the (Co,Cu,Mg,Ni,Zn)O compound.

Received 21st January 2026,
Accepted 22nd April 2026

DOI: 10.1039/d6ma00097e

rsc.li/materials-advances

1. Introduction

Due to their highly tailorable functional properties, there is increasing interest in high entropy ceramics and, particularly, in the area of entropy-stabilized oxides. This was first reported in a seminal paper by Rost *et al.*,[1] that explored the rock-salt composition (Co,Cu,Mg,Ni,Zn)O [Note†]. In the last few years, many other structures of complex composition oxides, including "high entropy oxide materials",[2,3] were obtained. Several reviews were published discussing the structures, the extent of chemical substitutions and some functional properties of these new materials.[4–13] However, this canonical rock-salt composition continued to be the most studied.[14–25]

An entropy stabilized phase is, as the name suggests, a compound whose structure (meta)stability is determined by the configurational entropy.[26–29] However, as recent studies have emphasized,[22,23,30,31] challenging aspects related to the phase stability criteria, as well as to the basic understanding of the point defect formation in the entropy-stabilized oxide (Co,Cu,Mg,Ni,Zn)O in relation to the local configuration and structural distortion are still under debate. In addition, the effective role of entropy in the stabilization should be demonstrated for each system,[23] and even for (Co,Cu,Mg,Ni,Zn)O.

The focus of the present work is on the prototypical entropy stabilized oxide of composition $Co_{0.2}Cu_{0.2}Mg_{0.2}Ni_{0.2}Zn_{0.2}O$, hereafter noted (Co,Cu,Mg,Ni,Zn)O, and in particular on the thermodynamic functions related to the formation and stability of this material. Due to the complexity of the relationship between different compositional variables and properties of multicomponent oxide systems, the fundamental understanding of the chemical processes involved is still limited. Even though it has been emphasized that the phase formation is

[a] *Institute of Physical Chemistry – Ilie Murgulescu of the Romanian Academy, Splaiul Independentei 202, 060021 Bucharest, Romania.*
E-mail: speranta.tanasescu@gmail.com, stanasescu2004@yahoo.com, stanasescu@icf.ro
[b] *ICMMO (UMR 8182 CNRS), Université Paris-Saclay, 91405 Orsay, France.*
E-mail: nita.dragoe@universite-paris-saclay.fr

† According to the IUPAC convention, the cations should be named in the alphabetical order (International Union of Pure and Applied Chemistry, Quantities, Units and Symbols in Physical Chemistry, Second edition 1993).

correlated with the energetics of the competing phases, the thermodynamics and mechanisms underlying the phase transformations induced by the phase metastability are of great interest.[26,32] Such analyses need robust, detailed and precise thermodynamic data, because the driving forces for chemical reactions and diffusion can be given properly in terms of thermodynamic properties.

In the present paper the relevant functions suitable for evaluation of the thermodynamic stability in particular temperature ranges associated with structural changes during heating have been measured. The energetic parameters obtained in a large temperature range using several pertinent methods (drop calorimetry, TG/DSC, and electromotive force measurements) together with the thermal expansion and electrical conductivity data have been analyzed and the relationship of the thermodynamic stability with changes in the defect structure in the (Co,Cu,Mg,Ni,Zn)O sample is discussed.

We report here, for the first time, the thermodynamic data of oxygen dissolution for the (Co,Cu,Mg,Ni,Zn)O samples. They have a strong dependence on temperature and show significant variations in the temperature range where the charge imbalance is mainly compensated by the formation of oxygen vacancies. The oxygen vacancy ordering also shows contribution to the observed phenomena. Through a combined analysis of microstructure and thermodynamic data, the correlative effects of temperature and defect structures on the thermodynamic behavior of the (Co,Cu,Mg,Ni,Zn)O sample have been discussed. Moreover, the distinct thermomechanical (TMA) behavior suggests a strong correlation between the thermal expansion and the energetic parameters. It can also be correlated with the mass change observed from TG data during the transition to the single-phase rock-salt structure and is supported by the thermodynamic properties of oxygen dissolution in the (Co,Cu,Mg,Ni,Zn)O oxide structure obtained by using the solid electrolyte electrochemical cells method.

It was also shown that the evolution of the partial molar thermodynamic data of the oxygen dissolution correlates well with the variation of the electrical conductivity with temperature and confirms the strong interplay between the thermodynamic properties and electrical and structural characteristics. Based on these results, it is possible to find new routes for modifying the properties of these materials using various substitutions by several aliovalent elements, and creating vacancies in the oxygen sites. Thus, the thermodynamics approach of the interplay between structural characteristics and energetic mechanisms underlying the phase transformations is a key issue when searching for both scientific and applicative reasons.

2. Experimental

2.1. Synthesis

The samples were prepared by standard solid-state synthesis from high purity oxides MgO (Alfa Aesar 99.95%), CuO (Alfa Aesar 99.7%), NiO (Strem Chemicals 4N), Co_3O_4 (Alfa Aesar 99.7%) and ZnO (Alfa Aesar 4N). The powders were mixed in stoichiometric cation ratios in a Fritsch Pulverisette ball mill in a 20 mL agate vial with agate balls. The homogeneous mixture was then pressed uniaxially under 250 MPa into 12 × 3 × 3 mm^3 bars. 24 bars were obtained from the same mixture and heated in air for 12 hours at 1000 °C in alumina crucibles with a heating rate of 200 °C h^{-1}. After the thermal treatment, the samples were quenched to room temperature in air. Powder XRD was performed by using a Panalytical X'Pert diffractometer with a Johansson Ge(111) incident monochromator (Cu-K_{a1} radiation) and X'celerator detector. The diffraction patterns are consistent with previous reports[1,4,5] and the samples have a well-defined rock-salt structure. The lattice parameter obtained by LeBail fit was 4.2381(3) Å and the R_{wp} was 6.7%, see Fig. S1 (SI).

2.2. Measurements by drop calorimetry

The enthalpy increments $H_T - H_{298}$ of the sample in the isothermal regime were investigated by drop calorimetry using a multidetector high temperature calorimeter (MHTC-96) of SETARAM working in the drop mode. The procedure was described in detail in previous papers.[33,34] (Co,Cu,Mg,Ni,Zn)O samples in the form of small pellets weighing about 50 mg, accurately measured by a Mettler-Toledo microbalance to ±2 × 10^{-6} g, were used. The experiments consist in dropping the sample kept at room temperature (T_0) into a pure α-alumina bed maintained at a desired temperature in the calorimeter block. The temperature is measured to be $T \pm 0.1$ K with a calibrated thermocouple (Pt–Rh 30% − Pt–Rh 6%). The temperature calibration was carried out separately by heating pure standard metals (In, Sn, Pb, Zn, Al, Ag). The sample dropping is alternated by a reference of α-alumina standard (Standard Reference Material – SRM 720), under identical experimental conditions. The sensitivity of the calorimeter was deduced by comparing the heat exchange with the data given by the NIST [Note‡] for α-Al_2O_3. Our results with sapphire all agree within 0.15% with NIST values. Measurements were performed in an argon atmosphere, in the temperature range of 873–1273 K, at prefixed temperature steps of 25 K. The heat flux was recorded as a function of time. The peak area (after subtracting the baseline) associated with each drop corresponds to the respective enthalpy increment, $H_T - H_{298}$. The baseline treatment and the peak integration were carried out automatically by data acquisition and processing using the Setsoft software supplied by SETARAM. The enthalpy increments measured for each temperature step were calculated by averaging the values of at least six individual samples and SRM drops. A maximal uncertainty of 2%, expressed with a 95% confidence interval was obtained. Enthalpy increment values for the (Co,Cu,Mg,Ni,Zn)O material have not been previously reported in the literature.

2.3. DSC/TG analysis

The thermal behavior of the processed samples in a non-isothermal regime was investigated by simultaneous

‡ NIST (National Institute of Standards and Technology).

differential scanning calorimetry (DSC) and thermogravimetry (TG) using Setaram SETSYS Evolution 17 equipment. Samples contained in alumina crucibles were heated from room temperature to 1273 K under a constant flow of 16 mL min^{-1} of pure argon and at a heating rate of 5 K min^{-1}. Before each heating run, the specimen chamber was purged with high purity argon for about 15 min. The sample mass for DSC measurements was about 18 mg. The thermo-analyzer calibration was performed using standard metallic substances in the whole temperature range of the experiment with a 5 K min^{-1} heating rate, with the same type of crucible used for the experiments (alumina crucibles) and with the same carrier gas (Ar with high purity). The onset melting point temperatures and heats of fusion of 99.99% purity standard metallic materials (In, Sn, Pb, Zn, Al, Ag, and Au) were used for temperature correction and energy calibration.[35,36] Multiple runs under identical conditions were performed to check the data reproducibility. The error of TG measurement is ±0.15%. The measured transformation temperature is accurate to ±2 K; the transformation enthalpy is at best accurate to ±5%. To calculate enthalpy variation and mass change, the Calisto-AKTS software was used.

2.4. Thermomechanical analysis (TMA)

Thermal expansion of the sample associated with the structural changes was investigated by using a Thermomechanical Analyzer SETSYS Evolution TMA calibrated to a quartz standard. The sample powder was pressed into pellets of 6 mm diameter and 1.3 mm height. A force of 0.049 N was applied to the sample in order to provide good contact between the apparatus probe and the specimen. Thermal expansion measurements were performed at a heating rate of 5 K min^{-1} over the range 298–1373 K and in an argon atmosphere.

2.5. Solid state electromotive force measurements (EMF) coupled with solid state coulometric titration

In order to further evaluate the thermodynamic data, the thermodynamic properties represented by the relative partial molar free energies, enthalpies and entropies of oxygen dissolution in the crystalline phase ($\Delta\bar{G}_{O_2}$, $\Delta\bar{H}_{O_2}$, ΔS_{O_2}), as well as the equilibrium partial pressures of oxygen ($\log p_{O_2}$) were obtained in the temperature range of 823–1273 K by using the solid electrolyte electrochemical cells method. As shown in previous papers,[37–39] the thermodynamic stability limits of the multicomponent-type oxides are conveniently situated within the range of oxygen chemical potentials that can be measured using galvanic cells containing 12.84 wt% yttria stabilized zirconia solid electrolyte and an iron-wüstite reference electrode. The design of the apparatus, as well as the theoretical and experimental considerations related to the applied method have been described previously.[38,39] Measurements were performed in vacuum at a residual gas pressure of 10^{-5} Pa, at 50 K intervals, each time waiting until equilibrium conditions were obtained. The overall uncertainty due to the temperature and potential measurement (taking into account the overall uncertainty of a single measurement and also the quoted accuracy of the voltmeter) was ±1.5 mV. This was equivalent to ±0.579 kJ mol^{-1} for the free energy change of the cell. Considering the uncertainty of ±0.523 kJ mol^{-1} in the thermodynamic data for the iron-wüstite reference,[40–43] the overall data accuracy in oxygen potential measurement was estimated to be ±1.6 kJ mol^{-1}.

The free energy change of the cell is given by the expression:

$$\Delta G_{cell} = \mu_{O_2} - \mu_{O_2}(ref) = 4FE \quad (1)$$

where μ_{O_2} and $\mu_{O_2}(ref)$ are, respectively, the oxygen chemical potentials of the sample and the reference electrode, F is the Faraday constant ($F = 96.5 \times !0^3$ C mol^{-1}) and E is the steady state EMF of the cell in volts (where 1 V = 1 J C^{-1}). By using the experimental values of the electromotive force of the cell and knowing the free energy change of the reference electrode, the values of the relative partial molar free energy of the solution of oxygen in the crystalline phase $\Delta\bar{G}_{O_2}$ and hence the pressures of oxygen in equilibrium with the solid p_{O_2} can be calculated knowing the temperature T and the gas constant R:

$$\Delta\bar{G}_{O_2} = RT\ln p_{O_2} \quad (2)$$

The relative partial molar enthalpies $\Delta\bar{H}_{O_2}$ and entropies $\Delta\bar{S}_{O_2}$ were obtained according to the known relationships:[38,39]

$$\frac{\partial\frac{\Delta\bar{G}_{O_2}}{T}}{\partial T} = -\frac{\Delta\bar{H}_{O_2}}{T^2} \quad (3)$$

$$\Delta\bar{G}_{O_2} = \Delta\bar{H}_{O_2} - T\Delta\bar{S}_{O_2} \quad (4)$$

Following the completion of the steady state measurements in the whole range of temperatures, by solid state coulometric titration the precise change of the oxygen stoichiometry of the sample was obtained[38,39] by using a Bi-PAD Tacussel Potentiostat. The titrations were performed *in situ* at 1123 K at a pressure of 10^{-5} Pa. According to Faraday's law, the mass change (g) of the sample is related to the transferred charge Q (A s) by:

$$|\Delta m| = 8.291 \times 10^{-5}Q \quad (5)$$

The resolution in measuring mass changes in this manner is extremely high compared with the use of typical mass balances (1 A s corresponds to $\sim 8 \times 10^{-5}$ g). After the desired amount of charge was passed through the cell, the current circuit was opened and sufficient time (about three hours) had to be allowed for the electrode to equilibrate. Practically, we considered that EMF had reached its equilibrium value when three subsequent readings at 30 min intervals varied by less than 0.5 mV. After the sample reached equilibrium, for the new obtained composition, the temperature was changed under open-circuit conditions, and the equilibrium EMFs for different temperatures between 1123 and 1273 K were recorded.

2.6. Electrical conductivity

The electrical conductivities were measured by AC impedance spectroscopy. The measurements were carried out with the Solartron Analytical 1255A using a ProboStat sample holder (NorECs) heated up by an Elite TSV12/50/300 furnace. The

impedance spectroscopy measurements were conducted in air, in the temperature range of 723–1273 K, over the frequency range of 100 Hz–1 MHz; the amplitude of the alternative signal was 1 V. The temperature was acquired by using a Pt–Rh thermocouple located close to the sample. For good contact with the electrodes, two Pt electrodes were pasted onto the sample surfaces and fired at 573 K for 1 hour.

3. Results and discussion

A proper understanding of the competition between the enthalpy-dominated multi-phase state and an entropy-dominated single-phase state is central to describing metastable to single phase transformation in (Co,Cu,Mg,Ni,Zn)O. The temperature sensitivity of entropy leads to metastability of the entropy-driven state resulting in a reversible entropic phase transformation.[44,45] A great deal of effort has been devoted in recent years to investigating this continuum of phase heterogeneity (also named the "phase spectrum"),[7] by considering different composition variables (by changing the elemental composition, the fraction of the constituent elements, grain sizes, and using different methods of synthesis).[4,14,17,22,46] In the present paper, we provide insights for the first time into the thermodynamic parameters obtained by a couple of measurements – in both isothermal and dynamic regimes – describing this metastable to single phase transformation in (Co,Cu,Mg,Ni,Zn)O which is regulated by temperature.

3.1. Evaluation of the relative enthalpies and related thermodynamic functions of the (Co,Cu,Mg,Ni,Zn)O compound by drop calorimetry

The basic drop calorimetry data, namely the enthalpy increments ($H_T - H_{298}$) in the temperature range of 323–1098 K are shown in Fig. 1.

One can observe that the enthalpy increment variation with temperature is nonlinear in nature, some features being noticed firstly around 1023 K and then between 1123 and 1173 K with a most pronounced heat anomaly at 1148 K. The change of the slope in the enthalpy – temperature variation of our sample suggests the structural changes accompanied by the temperature dependent evolution of the energetic parameters. A marked change of slope between 1173 and 1273 K (inset of Fig. 1) should be noted. With increasing temperature, the considerable defect-induced contributions to the overall thermal behavior have to be taken into consideration.

To further evaluate these results, the heat contents were expressed as an explicit temperature function f (T) for the temperature ranges 923.15–1023.15 K, 1048.15–1123.15 K and 1173.15–1223.15 K and least squares fitted into polynomial equations of the form:

$$H_T - H_{298} = a + bT + cT^2 \quad (6)$$

The values of the coefficients a, b, and c are given in Table 1 together with the standard error in the temperature ranges of measurements.

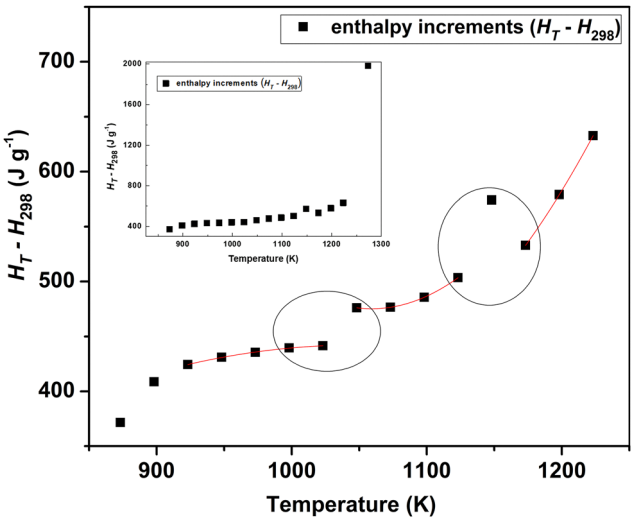

Fig. 1 Temperature dependence of the experimental enthalpy increments ($H_T - H_{298}$). The continuous lines were obtained by fitting the data to a second-order polynomial form described in eqn (6).

The temperature-dependent estimates of the heat capacity were obtained by differentiating above enthalpy increment equations with respect to temperature:[34,47]

$$C_p = \frac{\partial}{\partial T}(H_T - H_{298}) \quad (7)$$

The relative entropy (the entropy increment) is obtained by integrating the heat capacity data at constant pressure:

$$S_T - S_{298} = \int_{298}^{T} \frac{C_p}{T} dT \quad (8)$$

Using the fundamental thermodynamic relationship: $\Delta G = \Delta H - T\Delta S$, the relative Gibbs energy function ($G_T - G_{298}$) is calculated by combining the measured enthalpy increment and the calculated entropy increment. The thermodynamic functions obtained by processing the calorimetric data are included in Table 2. Taking into account the systematic error related to the uncertainties in the temperature measurements, as well as in the enthalpy data, the general overall uncertainty is estimated to be around 0.2% for the heat capacity and the thermodynamic functions. Enthalpy increment and thermodynamic functions values for (Co,Cu,Mg,Ni,Zn)O oxide materials have not been previously reported in the literature for comparison.

It is of special interest for us to show how the thermodynamic parameters may be used to understand the particularities of the structure behavior upon heating. One can observe that the increasing trend of the specific heat capacities with the temperature increase is accompanied by the increasing values of the entropies (Table 2), the larger values being noted at temperatures between 1173 and 1223 K. The changes that appear in the variation of entropy around the temperatures of 1023 and 1123 K highlight the progressive multiphase to single phase transition that occurs at these temperatures.[1,24] Also, the tendency of the rock-salt structure to distort from the cubic

Table 1 Values of the fit coefficients in eqn (6)

	Fitting parameters		
Temperature domain (K)	*a*	*b*	*c*
923.15–1023.15 K	-809.14 ± 118.95	2.39 ± 0.245	$-1.14 \times 10^{-3} \pm 1.25\times 10^{-4}$
1048.15–1123.15 K	8245.29 ± 88.85	-14.67 ± 0.16	$0.0069 \pm 7.5 \times 10^{-5}$
1173.15–1223.15 K	6875.029 ± 0	-12.50 ± 0	$6.05 \times 10^{-3} \pm 0$

The values after the "±" sign correspond to the standard error of estimates which is a measure of the scatter about the regression curve.

Table 2 Thermodynamic functions of the (Co,Cu,Mg,Ni,Zn)O sample

T (K)	C_p (J g^{-1} K^{-1})	$S_T - S_{298}$ (J g^{-1} K^{-1})	$G_T - G_{298}$ (kJ g^{-1})
923	0.28	0.32	0.13
948	0.23	0.26	0.18
973	0.17	0.20	0.24
998	0.11	0.14	0.29
1023	0.05	0.07	0.37
1048	0.54	0.68	−0.24
1073	0.56	0.71	−0.29
1098	0.57	0.75	−0.34
1123	0.59	0.78	−0.37
1173	1.69	2.31	−2.18
1198	1.99	2.77	−2.74
1223	2.29	3.24	−3.33

symmetry decreases when passing 1123 K, which corresponds to a higher disorder.[15,32] In line with this idea, the larger entropies increment obtained in the 1173–1223 K interval for the (Co,Cu,Mg,Ni,Zn)O sample is characteristic of the higher degree of internal disorder. At the same time, the large negative values of the free energy, observed in this temperature range, highlight more stable states in the samples with the rock-salt structure. The present data obtained for the first time for (Co,Cu,Mg,Ni,Zn)O support the previous findings related to an entropy-driven solid–solid transformation.[1,14,24]

3.2. DSC/TG

In order to further evaluate the heat effects related to the anomalies evidenced by drop calorimetry, the thermal behaviour of the (Co,Cu,Mg,Ni,Zn)O material was investigated under a non-isothermal regime by simultaneous thermogravimetry (TG) and differential scanning calorimetry (DSC). The TG and DSC plots of the as-prepared (Co,Cu,Mg,Ni,Zn)O sample are shown in Fig. 2.

An endothermic thermal effect with a maximum at ~ 1140 K was noted on the DSC curve, which could be correlated with the transition to the rock-salt structure. As reported by Rost *et al.*,[1] an intense 111 rock-salt peak in the diffraction data in the temperature interval between 1098 K and 1148 K was observed. The maximum temperature of the thermal effect on the DSC curve is in good agreement with the heat anomaly indicated by drop calorimetry between 1123 and 1173 K, both measurements being performed in Ar. On the TG curve, a mass loss of 0.5% at the temperature range of 1021 K and above, corresponding to the endothermic effect was observed. According to previous reports,[1,11,14,24] this could be due to the release of oxygen following the formation of doubly ionized oxygen

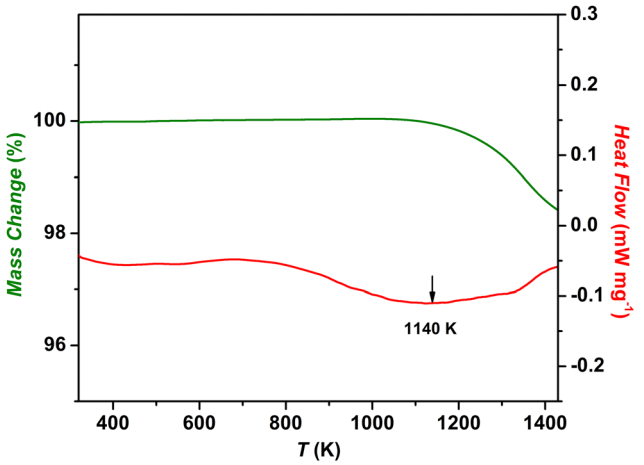

Fig. 2 TG and DSC plots of the as-prepared (Co,Cu,Mg,Ni,Zn)O sample.

vacancies which is expressed by the equation: $O_O \Rightarrow V_O^{\bullet\bullet} + 2e' + 1/2O_2$ where O_O, $V_O^{\bullet\bullet}$, and e' represent (according to Kroger–Vink notation)[48] the oxygen ions at their normal positions, oxygen site vacancies, and generated electrons, respectively. This suggests a correlation between molecular oxygen evolution (particularly the oxygen stoichiometry of the sample), mass loss, and the endothermic effect registered by DSC measurements. While the magnitude of the mass loss at temperatures below 800 K and thus the change in corresponding oxygen stoichiometry can be regarded as negligible, the stoichiometry deviation in (Co,Cu,Mg,Ni,Zn)$O_{1-\delta}$ associated with this endothermic event was calculated to be δ = 0.022. By increasing the heating rate to 10 K min^{-1} (see the SI, Fig. S2), when keeping the same working atmosphere (continuously flowing Ar), a minor shift in the onset temperature of only 3 K toward higher temperatures and a mass loss of 0.38% were observed. The corresponding stoichiometric deviation of the sample was calculated as δ = 0.017, which is very close to the δ value obtained at a heating rate of 5 K min^{-1} ($\Delta\delta$ = 0.005). The obtained results on the change in oxygen stoichiometry in the particular temperature range associated with the mass change, not only support the thermal behavior of the sample when working in a dynamic regime, but also correlate with the trend in the temperature dependence of enthalpy increments measured by drop calorimetry around 1123 K. This important issue related to the correlative effects of temperature and defect structure on the thermodynamic behavior of the (Co,Cu,Mg,Ni,Zn)O sample will be later discussed in this paper based on

the evaluation of thermodynamic data of oxygen dissolution in the solid oxide structure obtained by EMF measurements (in Section 3.4).

3.3. Thermomechanical analysis (TMA)

A direct relationship between the lattice strains and the point defects in the lattice has been previously pointed out for different entropy-stabilized materials.[11,17,19,49–51] For the oxide, the distortion on the lattice is concentrated on the anion sublattice, which is consistent with the experimental results of Rost.[52] This distortion creates the possibility of interphase stresses and anticipates the change of the thermal expansion coefficients in the two different phase regions.

In order to elucidate this point further, we considered the relative length change of the (Co,Cu,Mg,Ni,Zn)O sample associated with structural changes during heating (Fig. 3). A linear increase of the relative length of the sample with temperature is observed from room temperature up to 973 K.

Then, two small anomalies in the displacement variation could be noted: a relative length change of ~0.28% obtained between 973 K and 1100 K, with a shrinkage maximum at 1034 K, and a length change of ~0.30% between 1120 K and 1223 K with a maximum in the shrinkage at 1210 K. We note that the thermal expansion measured at a constant heating rate includes a decomposition of the metastable phase toward a mixture of oxides. After 1223 K, the relative length of the sample linear increases again with the temperature, but with a marked change of the displacement slope. In addition, the enhancement to 48.8×10^{-6} K^{-1} of the average thermal expansion coefficient (CTE) determined from our data is observed over the temperature range 1223–1273 K which is around the temperatures where the larger enthalpy increments were obtained from calorimetric measurements. This distinct thermomechanical behavior speaks in favour of the strong correlation between the thermal expansion and the energetic parameters. It can also be correlated with the mass change observed from TG data associated to the changes in the defect structure on the anion sublattice and is supported by the following thermodynamic properties of oxygen dissolution in the HEO oxide structure obtained by using the solid electrolyte electrochemical cells method.

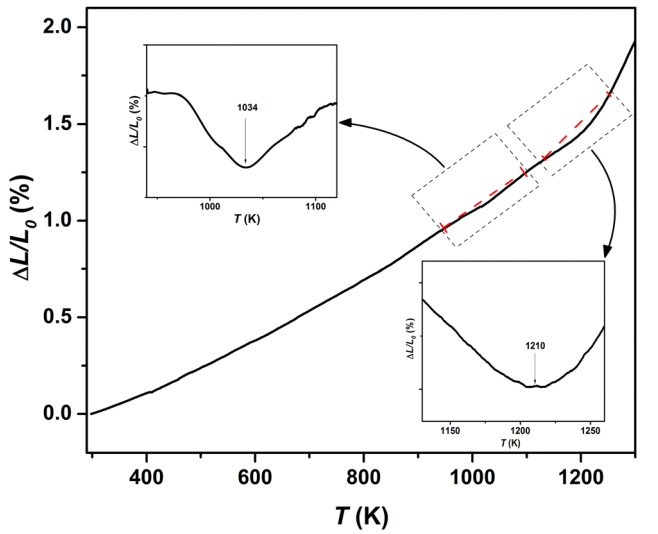

Fig. 3 Thermal expansion as a function of temperature of the (Co,Cu,Mg,Ni,Zn)O specimen.

3.4 Thermodynamic properties of oxygen dissolution in the crystalline phase by using solid electrolyte electrochemical cells

Previous studies have shown that many oxides of transition metals with a rock-salt structure have a strong tendency to non-stoichiometry, and thus the point defects resulting by the charge compensation mechanism could be taken into account.[4,6,11,17,19,44,53] Moreover, some reports stated that the predominant disorder is present in the anion sublattice of (Co,Cu,Mg,Ni,Zn)O oxide.[5,6] Bérardan *et al.*[15] showed that in the presence of Cu^{2+} in octahedral coordination, the Jahn–Teller effect could lead to a local deformation of the oxygen sublattice around copper ions in order to decrease the overall energy of the crystal. In addition, the (Co,Cu,Mg,Ni,Zn)O compound with multivalent cations may experience a thermodynamic dependence on oxygen chemical potential (or oxygen partial pressure),[6,11,54,55] potentially leading to charged defects. Previous defect studies as a function of p_{O_2}[6] suggest potential larger oxygen vacancy concentrations than is typical for the end-member oxides, without observable phase decomposition.

In order to get a better understanding of how the thermodynamic properties are related to the oxygen content in the present (Co,Cu,Mg,Ni,Zn)O material, the thermodynamic properties represented by the relative partial molar free energies $\Delta\bar{G}_{O_2}$, enthalpies $\Delta\bar{H}_{O_2}$ and entropies $\Delta\bar{S}_{O_2}$ of oxygen dissolution in this complex solid oxide structure, as well as the equilibrium partial pressures of oxygen were obtained (eqn (1)–(4)) in the temperature range of 823–1273 K by using the solid electrolyte electrochemical cells method. The thermodynamic data of oxygen in the oxide can be interpreted to describe the defect structure considering that partial molar energies are being correlated with the concentration of the oxygen vacancies, $\Delta\bar{H}_{O_2}$ can be regarded as a measure of the binding strength of O^{2-} in the oxide and $\Delta\bar{S}_{O_2}$ as a measure of O^{2-} ordering in the oxide. The set of experimental outcomes obtained by EMF measurements help to complete our thermodynamic understanding of the oxygen defects contribution to the entropy driven transition from multiple-phase to single phase in the (Co,Cu,Mg,Ni,Zn)O sample. Moreover, to our best knowledge, there are no other studies reporting these data available in the literature.

The partial molar free energies ($\Delta\bar{G}_{O_2}$) and the corresponding $\log p_{O_2}$ values for the (Co,Cu,Mg,Ni,Zn)O sample are shown in Fig. 4. One can observe that the variation of the partial molar free energy with temperature is not monotonous. The partial molar energy increases with increasing temperature until 973 K, then a slight change of the slope is noted between 973 K and 1023 K. Between 1023 and 1123 K, $\Delta\bar{G}_{O_2}$ increases again with temperature until 1173 K. After 1173 K, the partial molar energy decreases with increasing temperature to 1273 K. The same trend is accounted for the $\log p_{O_2}$ variation, which

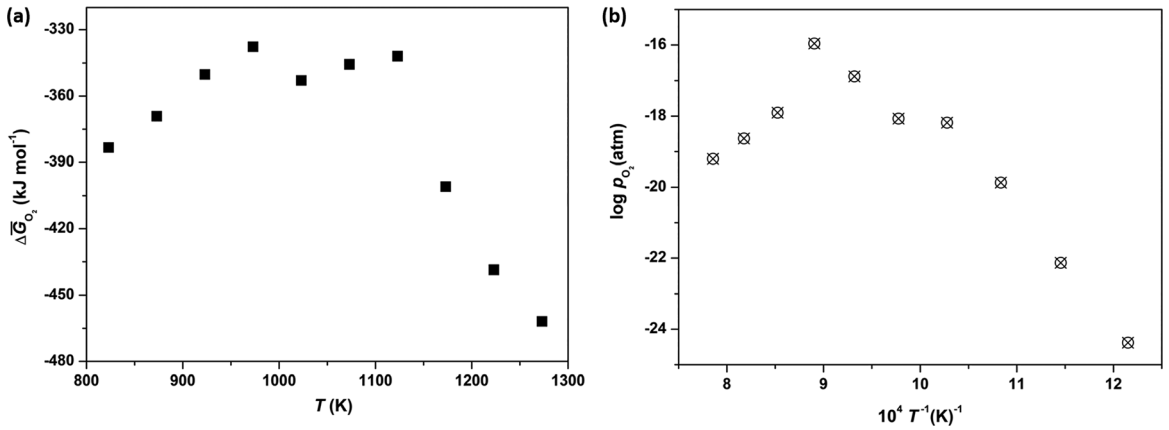

Fig. 4 Variation of (a) $\Delta\bar{G}_{O_2}$ and (b) $\log p_{O_2}$ with temperature.

presents a marked decrease after 1173 K. Thus, after 1173 K, the sample exhibits the lowest partial molar free energy showing increased stability. If the partial molar energies are correlated with the concentration of the oxygen vacancies, we obtain that the sample is thermodynamically more stable between 1173 and 1273 K when the concentration of oxygen vacancies is lower.

Further clarification could be achieved by determining the $\Delta\bar{H}_{O_2}$ and $\Delta\bar{S}_{O_2}$ values in the temperature ranges where the partial molar free energy is a linear function of temperature (Table 3). In these temperature ranges, the partial molar entropies and enthalpies are independent of temperature.

The partial molar enthalpy and entropy values increase with the increasing temperature, suggesting a decrease in the binding energy of oxygen and a decrease of order in the oxygen sublattice of the (Co,Cu,Mg,Ni,Zn)O structure, respectively. Due to the large increase in $\Delta\bar{S}_{O_2}$ in the temperature range of 1173–1273 K, it is probable that the oxygen vacancies are not distributed to some particular oxygen sites but they are randomly distributed, supporting the previous findings related to an entropy-driven phase transformation.[1] The results are also in agreement with our data obtained by drop calorimetry regarding the higher degree of internal disorder in this temperature range.

In addition, the thermodynamic behavior of the analyzed sample (both before 1173 K and after this temperature) is in agreement to the reported simulation data,[31,56] regarding the energy of oxygen vacancies formation (E_{vf}) in (Co,Cu,Mg,Ni,Zn)O which was found to be strongly dependent on the local configuration. The local lattice distortion due to the presence of Cu reduces E_{vf} leading to a higher concentration of oxygen vacancies after reduction. This is also sustained by our TG results in an Ar atmosphere showing the mass loss around 1100 K. After 1173 K, the tetragonally distorted phase vanishes as the material transitions to a stable single-phase cubic rock salt structure.[15,32,45] Increasing the energy of vacancy formation, a smaller concentration of oxygen vacancies (so, a lower partial molar energy) is expected, together with a higher partial molar entropy, as can be seen from Table 3 ($\Delta\bar{S}_{O_2}$ = 609.62 J mol^{-1} K^{-1}).

Table 3 Relative partial molar thermodynamic data of oxygen following heating the (Co,Cu,Mg,Ni,Zn)O sample between 823 and 1273 K

Temperature range (K)	$\Delta\bar{G}_{O_2} = \Delta\bar{H}_{O_2} - T\Delta\bar{S}_{O_2}$	
	$\Delta\bar{H}_{O_2}$ (kJ mol^{-1})	$\Delta\bar{S}_{O_2}$ (J mol^{-1} K^{-1})
823–973	−639.48 ± 15.19	−311.09 ± 16.89
1023–1123	−463.67 ± 21.55	−108.83 ± 20.07
1173–1273	311.75 ± 101.05	609.62 ± 82.58

Bérardan *et al.*[14] showed that the phase with the rock-salt crystal structure obtained for the (Co,Cu,Mg,Ni,Zn)O sample at high temperature will be preserved after air-quenching from 1273 K. This is why we want to check if the thermodynamic parameters for entropy-driven phase evidenced in our study under a nonoxidizing atmosphere will also be preserved by quenching under this condition. In Fig. 5, besides the behavior of the partial molar free energy when heated between 800 and 1273 K, the data obtained during the cooling of the sample are also depicted.

It is noted that upon cooling, the low values of $\Delta\bar{G}_{O_2}$ remain within the range typical for the entropy-driven phase transformation. This finding is significant for utilizing these materials in various applications such as energy production and storage,[12,57] electronics,[4,45] and catalysts.[8,58]

The $\Delta\bar{G}_{O_2}$ and $\log p_{O_2}$ data suggest a complex behavior occurring in (Co,Cu,Mg,Ni,Zn)O over the temperature range of 1123–1273 K. To further evaluate the previous results, the variation of the thermodynamic data of oxygen dissolution was analyzed by changing *in situ* the stoichiometry of the (Co,Cu,Mg,Ni,Zn)O sample at a constant temperature of 1123 K and in the pressure conditions of our experiment, namely at 10^{-5} Pa. The precise change of oxygen stoichiometry of $\Delta\delta = -0.005$ was performed by solid-state coulometric titration,[38,39] through cathodic reduction. After titration and equilibration, by changing the temperature under the open-circuit condition, the variation of EMF with temperature was again recorded for the new (Co,Cu,Mg,Ni,Zn)$O_{1-\delta}$ sample.

In Fig. 6, two sets of data before and after the isothermal titration experiments obtained in the temperature interval of

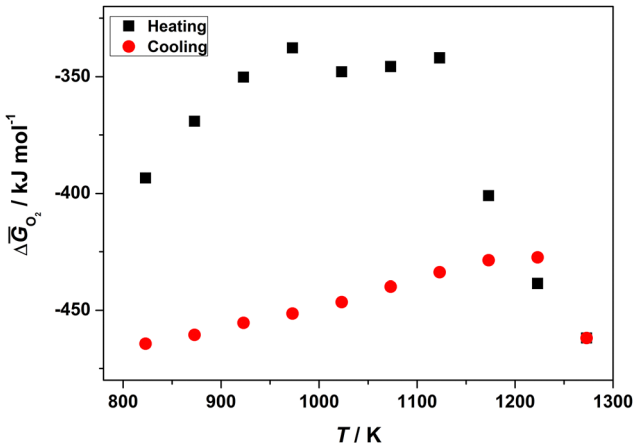

Fig. 5 Variation of $\Delta\bar{G}_{O_2}$ with temperature during heating and cooling of the (Co,Cu,Mg,Ni,Zn)O sample.

1123–1273 K are plotted. After titration, the $\Delta\bar{G}_{O_2}$ and $\log p_{O_2}$ values are decreasing which is indicative for the decrease of oxygen vacancy concentration. However, it was noted that their variation with temperature is not monotone and does not keep the same trend as before titration. The higher deviation with $\Delta\delta$ of the $\Delta\bar{G}_{O_2}$ and $\log p_{O_2}$ values are obtained at 1123 K and 1173 K. After 1173 K, the change in the $\Delta\bar{G}_{O_2}$ values for the (Co,Cu,Mg,Ni,Zn)$O_{1-\delta}$ sample likely accounts for their increase with temperature. This trend differs from that of the initial (Co,Cu,Mg,Ni,Zn)O sample, which shows the decrease in $\Delta\bar{G}_{O_2}$ values, indicating greater stability in this temperature range. Taking into account that the deviations from oxygen nonstoichiometry can significantly alter the oxygen storage capacity of these materials, the result should be important for a rational screening of new pure-phase entropy-stabilized materials by controlling the charge compensation mechanism and creating vacancies in the oxygen sites.

3.5. Electrical conductivity

In order to obtain further clarification on the relationship between the thermodynamic parameters and electrical conductivity behavior, the results of measurements of the conductivity of the (Co,Cu,Mg,Ni,Zn)O sample in the temperature range of 823–1373 K in air are presented in Fig. 7. We are particularly interested to observe the electrical conductivity behavior in this domain of temperature where the thermodynamic parameters are sensitive to both oxygen vacancies concentration and temperature.

The electrical conductivity of the sample increases with temperature, being linear in the particular temperature ranges related to the progressive multiphase to single phase transition, which is a typical behavior for a thermally activated process. The result is consistent with previous studies suggesting ''hopping small polarons'' as the mechanism responsible for electrical conductivity of the investigated (Co,Cu,Mg,Ni,Zn)O rock-salt material in air,[46,59,60] mechanism represented by the equation $\sigma = (\sigma_0/T)\exp(-E_a/kT)$ (where σ is the electrical conductivity, σ_0 is the pre-exponential factor, T is the absolute temperature, k is Boltzmann's constant, and E_a is the activation energy of conduction).

One can note that, even though the two types of measurements (thermodynamic and electrical measurements) are performed in different environmental conditions, the discontinuity in the conductivity upon heating in this temperature interval correlates with the behavior as a function of temperature of the thermodynamic data represented by partial molar free energy obtained by EMF measurements, with the discontinuity of enthalpy increment shown by drop calorimetry, as well as with the variation of thermal expansion coefficient. The state of oxygen vacancies, being ordered or disordered in the lattice together the considerable stress gradients developing in the materials due to the gradient in oxygen concentration have to be considered to explain the discontinuity in the conductivity and the lower energy of activation of E_a = 0.28 eV characteristic for the temperature window range 998–1048 K.

In the inset of Fig. 7 it is also presented the evolution of electrical conductivity in a larger temperature range including the lower temperature domain 373–773 K. The energy activation value of E_a = 0.84 eV obtained from our measurements in

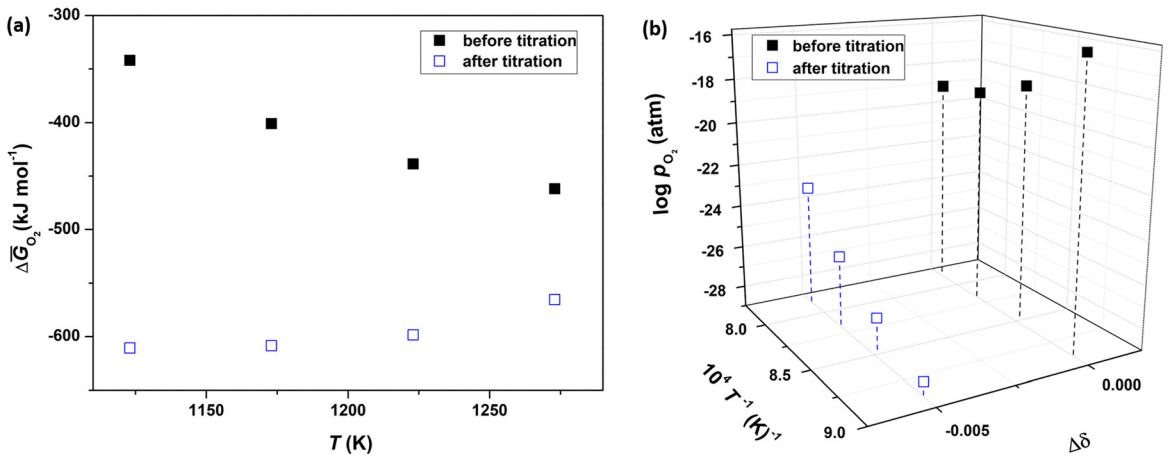

Fig. 6 Variation of (a) $\Delta\bar{G}_{O_2}$ and (b) $\log p_{O_2}$ with temperature and oxygen stoichiometry change ($\Delta\delta$ = −0.005).

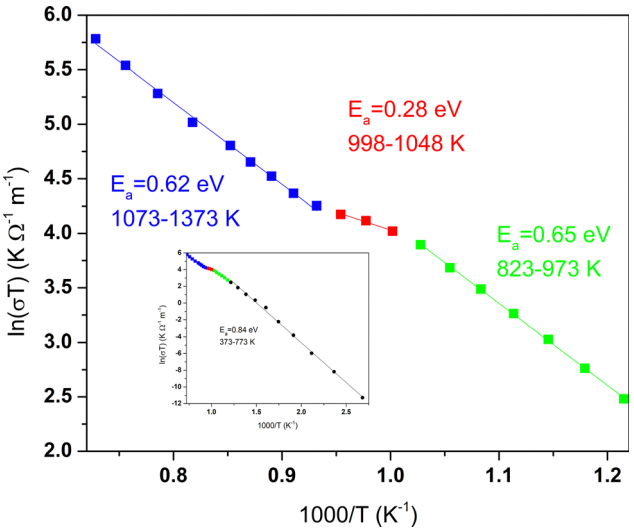

Fig. 7 Temperature dependence of the electrical conductivity of (Co,Cu,Mg,Ni,Zn)O in air between 823 and 1373 K. Inset: the temperature dependence of the electrical conductivity for the whole temperature range (373–1373 K).

this domain is quite close to the value of E_a = 0.80 eV obtained by Bérardan *et al.*[14] in the temperature window 313–373 K by considering the intrinsic resistance of the (Co,Cu,Mg,Ni,Zn)O specimen. The obtained values suggest that the energetically favorable long-range interactions between the charged defects that trap the oxygen vacancies become dominant at lower temperatures.

4. Conclusions

In the present paper the thermodynamic properties of the (Co,Cu,Mg,Ni,Zn)O entropy-stabilized compound have been investigated. For the first time, the relevant functions suitable for evaluation of thermodynamic stability in particular temperature ranges associated with structural changes during heating have been measured. The energetic parameters obtained from various measurements (Drop Calorimetry, TG/DSC, Electromotive Force Measurements) together with the thermal expansion and electrical conductivity data have been analyzed and the relationship of the thermodynamic stability with changes in the defect structure in the (Co,Cu,Mg,Ni,Zn)O sample has been revealed.

The enhanced values of the heat capacity and the larger entropies increment measured by drop calorimetry in the 1173–1223 K interval for the (Co,Cu,Mg,Ni,Zn)O sample are characteristic for the higher degree of internal disorder. At the same time, the large negative values of the free energy, observed in this temperature range, highlight more stable states in the samples with a rock-salt structure.

The maximum temperature of the thermal effect on the DSC curve is in good agreement with the heat anomaly between 1123 and 1173 K indicated by drop calorimetry.

The variation of the thermal expansion associated with the structural changes has been evidenced by thermomechanical measurements. The distinct thermomechanical behavior speaks in favour of the strong correlation between the thermal expansion and the energetic parameters. It can also be correlated with the mass change observed from TG data which was assigned to the release of oxygen associated to the oxygen vacancies formation and is supported by the thermodynamic properties of oxygen dissolution in the (Co,Cu,Mg,Ni,Zn)O oxide structure obtained by using the solid electrolyte electrochemical cells method.

The thermodynamic data of oxygen dissolution are reported for the canonical entropy-stabilized oxide for the first time. They have a strong dependence on the temperature, and show significant variations in the temperature range where the charge imbalance is mainly compensated by the formation of oxygen vacancies. The partial molar enthalpy and entropy values increase with increasing temperature, suggesting the decrease of the binding energy of oxygen and the decrease of order in the oxygen sublattice of the (Co,Cu,Mg,Ni,Zn)O structure, respectively. Due to the large increase in the temperature range of 1173–1273 K, it is considered that the oxygen vacancies would not be distributed to some particular oxygen sites but they are randomly distributed, supporting the previous findings related to an entropy-driven phase transformation.[1,14] The results are also in agreement with our data obtained by drop calorimetry regarding the higher degree of internal disorder in this temperature range. The analysis of the results obtained by combining the EMF measurements with solid-state coulometric titration allows for determining the role played by subtle oxygen stoichiometry changes in explaining the properties within the entropy-stabilized (Co,Cu,Mg,Ni,Zn)O sample.

We show that the evolution of the partial molar thermodynamic data of the oxygen dissolution correlates well with the variation of the electrical conductivity with temperature. Based on these results, it is possible to find new routes for modifying the properties of these materials using various substitutions by several aliovalent elements, and creating vacancies in the oxygen sites.

Further studies are in progress in our laboratory for a systematic investigation of the evolution of properties in compositions with different substitutions at the cation site.

Author contributions

F. T.: data curation, formal analysis, investigation, review & editing. C. M. investigation, methodology, writing – review & editing. A. S.: investigation, methodology, review & editing. A. B.-P.: investigation, review & editing. Cristian Hornoiu: investigation, methodology, review & editing. M.-C. L.: review & editing. F. M.: review & editing. D. B.: conceptualization, methodology, validation, visualization, writing – review & editing. N. D.: conceptualization, methodology, validation, visualization, writing – review & editing. S. T.: conceptualization, methodology, validation, visualization, formal analysis, supervision, project administration, resources, funding acquisition, writing – original draft, writing – review & editing.

Conflicts of interest

There are no conflicts to declare.

Data availability

The data that support the findings of this study are available from the corresponding author upon reasonable request.

Supplementary information (SI) is available. See DOI: https://doi.org/10.1039/d6ma00097e.

Acknowledgements

This work was performed under the Romanian Academy financed research program "Chemical Thermodynamics and Quantum Chemistry" and was made possible due to EU (ERDF) and Romanian Government contributions by acquisition of the research infrastructure under INFRANANOCHEM Project No. 19/01.03.2009 under POS-CCE O 2.2.1.

References

1 C. M. Rost, E. Sachet, T. Borman, A. Moballegh, E. C. Dickey, D. Hou, J. L. Jones, S. Curtarolo and J. P. Maria, *Nat. Commun.*, 2015, **6**, 8485.
2 M. Brahlek, M. Gazda, V. Keppens, A. R. Mazza, S. J. McCormack, A. Mielewczvk-Gryń, B. Musico, K. Page, C. Rost, S. B. Sinnott, C. Toher, T. Z. Ward and A. Yamamoto, *APL Mater.*, 2022, **10**, 110902.
3 B. L. Musicó, D. Gilbert, T. Z. Ward, K. Page, E. George, J. Yan, D. Mandrus and V. Keppens, *APL Mater.*, 2020, **8**, 040912.
4 D. Bérardan, S. Franger, A. K. Meena and N. Dragoe, *J. Mater. Chem. A*, 2016, **4**, 9536–9541.
5 N. Osenciat, D. Bérardan, D. Dragoe, B. C. Leridon, S. Holé, A. Meena, S. Franger and N. Dragoe, *J. Am. Ceram. Soc.*, 2019, **102**(10), 6156–6162.
6 Z. Grzesik, G. Smoła, M. Stygar, J. Dąbrowa, M. Zajusz, K. Mroczka and M. Danielewski, *J. Eur. Ceram. Soc.*, 2019, **39**, 4292–4298.
7 A. D. Dupuy, X. Wang and J. M. Schoenung, *Mater. Res. Lett.*, 2019, **7**(2), 60–67.
8 S. H. Albedwawi, A. Al Jaberi, G. N. Haidemenopoulos and K. Polychronopoulou, *Mater. Des.*, 2021, **202**, 109534.
9 A. Sarkar, R. Kruk and H. Hahn, *Dalton Trans.*, 2021, **50**, 1973–1982.
10 Y. Yao, F. Yang and X. Zhao, *J. Am. Ceram. Soc.*, 2022, **105**, 35–43.
11 G. N. Kotsonis, S. S. I. Almishal, F. Marques dos Santos Vieira, V. H. Crespi, I. Dabo, C. M. Rost and J.-P. Maria, *J. Am. Ceram. Soc.*, 2023, **106**, 5587–5611.
12 S. Schweidler, M. Botros, F. Strauss, Q. Wang, Y. Ma, L. Velasco, G. C. Marques, A. Sarkar, C. Kübel, H. Hahn, J. Aghassi-Hagmann, T. Brezesinski and B. Breitung, *Nat. Rev. Mater.*, 2024, **9**, 266–281.
13 C. Liu, S. Li, Y. Zheng, M. Xu, H. Su, X. Miao, Y. Liu, Z. Zhou, J. Qi, B. Yang, D. Chen, C.-W. Nan and Y.-H. Lin, *Prog. Mater. Sci.*, 2025, **148**, 101385.
14 D. Bérardan, S. Franger, D. Dragoe, A. K. Meena and N. Dragoe, *Phys. Status Solidi RRL*, 2016, **4**, 328–333.
15 D. Bérardan, A. K. Meena, S. Franger, C. Herrero and N. Dragoe, *J. Alloys Compd.*, 2017, **704**, 693–700.
16 A. Sarkar, R. Djenadic, N. J. Usharani, K. P. Sanghvi, V. S. K. Chakravadhanula, A. S. Gandhi, H. Hahn and S. S. Bhattacharya, *J. Eur. Ceram. Soc.*, 2017, **37**, 747–754.
17 M. Biesuz, L. Spiridigliozzi, G. Dell'Agli, M. Bortolotti and V. M. Sglavo, *J. Mater. Sci.*, 2018, **53**, 8074–8085.
18 X. Wang, J. Cortez, A. D. Dupuy, J. M. Schoenung and W. J. Bowman, *Mater. Res. Lett.*, 2023, **11**, 196–204.
19 T. D. Desissa, M. Meja, D. Andoshe, F. Olu, F. Gochole, G. Bekele, O. A. Zelekew, T. Temesgen, B. Brehane, K. D. Kuf and T. Hunde, *SN Appl. Sci.*, 2021, **3**, 733.
20 W. Hong, F. Chen, Q. Shen, Y.-H. Han, W. G. Fahrenholtz and L. Zhang, *J. Am. Ceram. Soc.*, 2019, **102**, 2228–2237.
21 K. C. Pitike, S. Kc, M. Eisenbach, C. A. Bridges and V. R. Cooper, *Chem. Mater.*, 2020, **32**, 7507–7515.
22 M. Coduri, L. R. Magnaghi, M. Fracchia, R. Biesuz and U. Anselmi-Tamburini, *Chem. Mat.*, 2024, **36**, 720–729.
23 M. Fracchia, M. Coduri, P. Ghigna and U. Anselmi-Tamburini, *J. Eur. Ceram. Soc.*, 2024, **44**, 585–594.
24 W. Mnasri, D. Bérardan, S. Tusseau-Nenez, T. Gacoin, I. Maurina and N. Dragoe, *J. Mater. Chem. C*, 2021, **9**, 15121–15131.
25 B. Yue, W. Dai, X. Zhang, H. Zhang, W. Zhong, B. Liu, S. Kawaguchi and F. Hong, *Scr. Mater.*, 2022, **219**, 114879.
26 S. J. McCormack and A. Navrotsky, *Acta Mater.*, 2021, **202**, 1–21.
27 S. Aamlid, M. Oudah, J. Rottler and A. M. Hallas, *J. Am. Chem. Soc.*, 2023, **145**(11), 5991–6006.
28 A. Sarkar, Q. Wang, A. Schiele, M. R. Chellali, S. S. Bhattacharya, D. Wang, T. Brezesinski, H. Hahn, L. Velasco and B. Breitung, *Adv. Mater.*, 2019, **31**(26), e1806236.
29 A. Sarkar, B. Breitung and H. Hahn, *Scr. Mater.*, 2020, **187**, 43–48.
30 M. Fracchia, M. Coduri, S. Bonati, C. Dejoie, P. Ghigna and U. Anselmi-Tamburini, *J. Eur. Ceram. Soc.*, 2025, **45**, 117237.
31 S. Chae, L. Williams, J. Lee, J. T. Heron and E. Kioupakis, *NPJ Comput. Mater.*, 2022, **95**, 8.
32 M. Fracchia, M. Coduri, M. Manzoli, P. Ghigna and U. Aselmi Tamburini, *Nat. Commun.*, 2022, **13**, 2977.
33 S. Tanasescu, A. Milea, O. Gîngu, F. Maxim, C. Hornoiu, S. Preda and G. Sima, *Phys. Chem. Chem. Phys.*, 2015, **17**, 28322–28330.
34 C. F. Rusti, V. Badilita, A. M. Sofronia, D. Taloi, E. M. Anghel, F. Maxim, C. Hornoiu, C. Munteanu, R. M. Piticescu and S. Tanasescu, *J. Alloys Compd.*, 2017, **693**, 1000–1010.
35 C. Marinescu, A. Sofronia, C. Rusti, R. Piticescu, V. Badilita, E. Vasile, R. Baies and S. Tanasescu, *J. Therm. Anal. Calorim.*, 2011, **103**, 49–57.
36 A. M. Sofronia, R. Baies, E. M. Anghel, S. Tanasescu and C. A. Marinescu, *Mater. Sci. Eng., C*, 2014, **43**, 153–163.

37 S. Tanasescu, Z. Yáng, J. Martynczuk, V. Varazashvili, F. Maxim, F. Teodorescu, A. Botea, N. Totir and L. J. Gauckler, *J. Solid State Chem.*, 2013, **200**, 354–362.
38 S. Tanasescu, N. D. Totir and D. I. Marchidan, *Electrochim. Acta*, 1998, **43**, 1675–1681.
39 S. Tanasescu, C. Marinescu, F. Maxim, A. Sofronia and N. Totir, *J. Solid State Electrochem.*, 2011, **15**, 189–196.
40 G. G. Charette and S. N. Flengas, *J. Electrochem. Soc.*, 1968, **115**, 796–804.
41 L. S. Darken and R. W. Gurry, *J. Am. Chem. Soc.*, 1945, **67**, 1398–1412.
42 C. E. Wicks and E. E. Block, *U. S. Bureau of Mines Bull.*, 1963, **605**, 57–58.
43 K. K. Kelley and E. G. King, *U. S. Bureau of Mines, Bull.*, 1961, **592**, 232.
44 A. D. Dupuy, M. R. Chellali, H. Hahn and J. M. Schoenung, *J. Mater. Res.*, 2023, **38**, 198–214.
45 A. D. Dupuy, I.-T. Chiu, P. Shafer, E. Arenholz, Y. Takamura and J. M. Schoenung, *J. Eur. Ceram. Soc.*, 2021, **41**(13), 6660–6669.
46 M. Balcerzak, K. Kawamura, R. Bobrowski, P. Rutkowski and T. Brylewski, *J. Electron. Mater.*, 2019, **48**, 7105–7113.
47 A. Milea, O. Gingu, S. Preda, G. Sima, C. Nicolicescu and S. Tanasescu, *J. Alloys Compd.*, 2015, **629**, 214–220.
48 F. A. Kroger and H. J. Vink, *Solid State Phys.*, 1956, **3**, 307–435.
49 L. K. Bhaskar, V. Nallathambi and R. Kumar, *J. Am. Ceram. Soc.*, 2020, **5**, 3416–3424.
50 H. Xiang, Y. Xing, F.-Z. Dai, H. Wang, L. Su, L. Miao, G. Zhang, Y. Wang, X. Qi, L. Yao, H. Wang, B. Zhao, J. Li and Y. Zhou, *J. Adv. Ceram.*, 2021, **10**, 385–441.
51 Z. Rak, C. M. Rost, M. Lim, P. Sarker, C. Toher, S. Curtarolo, J.-P. Maria and D. W. Brenner, *J. Appl. Phys.*, 2016, **120**(9), 095105.
52 C. M. Rost, Z. Rak, D. W. Brenner and J.-P. Maria, *J. Am. Ceram. Soc.*, 2017, **100**(6), 2732–2738.
53 Y.-M. Chiang D. P. Birnie and W. D. Kingery, *Physical Ceramics: Principles for Ceramic Science and Engineering*, John Willey, New York, 1996, ISBN: 978-0-471-59873-2.
54 Y. Zhong, H. Sabarou, X. Yan, M. Yang, M. C. Gao, X. Liu and R. D. Sisson Jr, *Mater. Des.*, 2019, **182**, 108060.
55 S. S. I. Almishal, M. Furst, Y. Tan, J. T. Sivak, G. Bejger, J. Petruska, S. V. G. Ayyagari, D. Srikanth, N. Alem, C. M. Rost, S. B. Sinnott, L.-Q. Chen and J.-P. Maria, *Nat. Commun.*, 2025, **16**, 8211.
56 O. Opetubo, T. Shen, R. Bordia and D. S. Aidhy, *Acta Mater.*, 2025, **296**, 121291.
57 A. Sarkar, R. Djenadic, D. Wang, C. Hein, R. Kautenburger, O. Clemens and H. Hahn, *J. Eur. Ceram. Soc.*, 2018, **38**(5), 2318–2327.
58 H. Cai, P. Zhang, B. Li, Y. Zhu, Z. Zhang and W. Guo, *Mater. Today Catal.*, 2024, **4**, 100039.
59 V. Jacobson, D. Diercks, B. To, A. Zakutayev and G. Brennecka, *J. Eur. Ceram. Soc.*, 2021, **41**, 2617–2624.
60 H. Vahidi, A. D. Dupuy, B. X. Lam, J. Cortez, P. Garg, T. J. Rupert, J. M. Schoenung and W. J. Bowman, *Adv. Funct. Mater.*, 2024, **34**, 2315895.